



A machine learning model for early detection of diabetic foot using thermogram images



Amith Khandakar^{a,b}, Muhammad E.H. Chowdhury^{a,*}, Mamun Bin Ibne Reaz^{b,**}, Sawal Hamid Md Ali^b, Md Anwarul Hasan^c, Serkan Kiranyaz^a, Tawsifur Rahman^a, Rashad Alfkey^d, Ahmad Ashrif A. Bakar^b, Rayaz A. Malik^e

^a Department of Electrical Engineering, Qatar University, Doha, 2713, Qatar

^b Dept. of Electrical, Electronics and Systems Engineering, Universiti Kebangsaan Malaysia, Bangi, Selangor, 43600, Malaysia

^c Department of Industrial and Mechanical Engineering, Qatar University, Doha, 2713, Qatar

^d Acute Care Surgery and General Surgery, Hamad Medical Corporation, Qatar

^e Weill Cornell Medicine-Qatar, Ar-Rayyan, Qatar

ARTICLE INFO

Keywords:

Thermogram
Diabetes mellitus
Diabetic foot
Convolutional neural network
Machine learning algorithms
Image enhancement techniques
Diagnostic utility

ABSTRACT

Diabetes foot ulceration (DFU) and amputation are a cause of significant morbidity. The prevention of DFU may be achieved by the identification of patients at risk of DFU and the institution of preventative measures through education and offloading. Several studies have reported that thermogram images may help to detect an increase in plantar temperature prior to DFU. However, the distribution of plantar temperature may be heterogeneous, making it difficult to quantify and utilize to predict outcomes. We have compared a machine learning-based scoring technique with feature selection and optimization techniques and learning classifiers to several state-of-the-art Convolutional Neural Networks (CNNs) on foot thermogram images and propose a robust solution to identify the diabetic foot. A comparatively shallow CNN model, MobilenetV2 achieved an F1 score of ~95% for a two-feet thermogram image-based classification and the AdaBoost Classifier used 10 features and achieved an F1 score of 97%. A comparison of the inference time for the best-performing networks confirmed that the proposed algorithm can be deployed as a smartphone application to allow the user to monitor the progression of the DFU in a home setting.

1. Introduction

Diabetes Mellitus (DM) leads to major complications such as heart disease, stroke, renal failure, blindness, and diabetic foot ulceration (DFU) with lower limb amputation [1]. Healing of DFU can be difficult or delayed [2] with an increased risk of infection and amputation [3]. DFU recurs in approximately 40% of patients after the first year and in 60% after three years [4,5] and leads to amputation in over 1 million diabetic patients annually in the USA [6]. In Europe, 250,000 diabetic patients undergo lower limb amputation with an associated mortality of 30% at one month and 50% at 1 year [7]. Diabetic foot ulceration is associated with markedly increased healthcare costs, decreased quality of life, infection, amputation, and death. The detection of patients at risk of DFU may enable timely intervention to prevent foot ulceration, amputation, and death.

Self-care via monitoring without medical assistance, for early signs of DFU, may allow timely offloading to prevent skin breakdown and development of a wound. Visual inspection has its limitations as people with obesity or visual impairment cannot see their site of ulceration. However, recent studies utilizing temperature monitoring have shown that they can predict the development of DFU in 97% of patients [4, 8–10]. Indeed, patients undergoing continuous foot temperature monitoring had a lower risk of DFU [11]. Skin temperature monitoring emerged during the 1970s, with “asymmetry analysis” proving to be very effective in identifying ulcers at an early stage [12]. A temperature difference of 2.22 °C (4°F) over at least two consecutive days could be used as a threshold for therapy to prevent DFU [8]. The system correctly identified the development of DFU in 97% of participants, with an average lead time of 37 days [13].

Thermography is a rapid non-invasive imaging technique to quantify

* Corresponding author.

** Corresponding author.

E-mail addresses: mchowdhury@qu.edu.qa (M.E.H. Chowdhury), mamun@ukm.edu.my (M.B. Ibne Reaz).

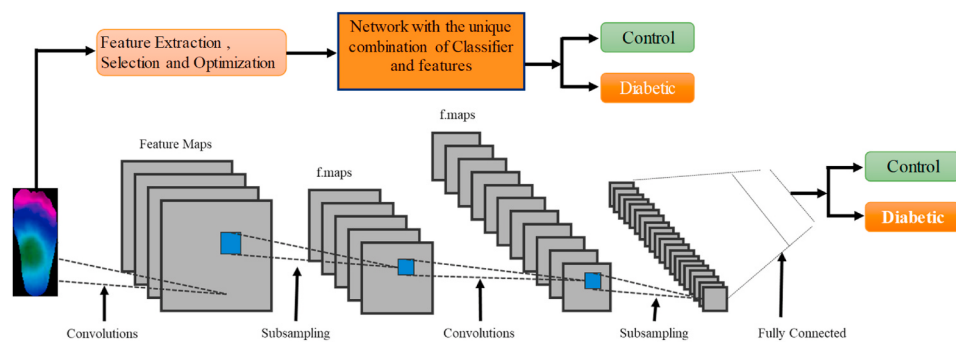


Fig. 1. Proposed classification pipeline using one-dimensional (1D) machine learning classifiers and 2-dimensional (2D) thermogram image.

thermal changes in the diabetic foot [13]. Several studies have proposed thermogram-based techniques for identifying those at risk of DFU [2,3, 14] by identifying a characteristic thermal distribution in the infrared image. The control group had a specific butterfly pattern [15] compared to a large variety of spatial patterns in the patients with diabetes [16, 17]. Whilst it is possible to assess thermal changes in one foot compared to the contralateral foot [18–21] if both feet have thermal changes without a butterfly pattern, then one foot cannot act as a reference.

Asymmetry cannot be measured despite a large temperature difference and identical spatial distributions in both feet. An alternative approach is to calculate the temperature change with respect to the butterfly pattern of a control group [22–24].

Machine learning (ML) techniques have been widely used for automatic image classification using feature extraction, feature ranking, and using different ML models, such as Artificial Neural Networks (ANN), k-nearest neighbors (KNN), and Support Vector Machines (SVM) [25–27].

Table 1
Statistical Analysis of 1D features for Binary Classification.

| | Item | Control | Diabetic | Total | Method | Statistic | P value |
|---|----------------------------|------------|--------------|------------|---------------|-----------|--|
| 1 | Gender | | | | | | |
| | • Male (%) | 58(64%) | 66(28%) | 124(37%) | | | |
| | • Female (%) | 32(36%) | 178(72%) | 210(63%) | | | |
| 2 | Age (Years) | | | | | | |
| | • N (missing) | 90(0) | 244(0) | 334(0) | Rank-sum test | 12.6108 | P < 0.05 (p-value = 1.84 × 10 ⁻³⁶) |
| | • Mean ± SD | 28 ± 8 | 55.98 ± 10.6 | 48.4 ± 16 | | | |
| | • Median | 25 | 55 | 52 | | | |
| | • Q1, Q3 | 23,30 | 50,63 | 34, 60 | | | |
| | • Min, Max | 21,52 | 23,84 | 21,84 | | | |
| 3 | Full-Foot Temperature (°C) | | | | | | |
| | • N (missing) | 90(0) | 244(0) | 334(0) | | | |
| | • Mean ± SD | 26.7 ± 1.6 | 29.7 ± 2.9 | 28.9 ± 2.9 | | | |
| | • Median | 26.8 | 30 | 28.8 | | | |
| | • Q1, Q3 | 25.9, 27.7 | 27.9, 32 | 26.6, 31.2 | | | |
| | • Min, Max | 22, 29.6 | 20.4, 35.6 | 20.4, 35.6 | | | |
| 4 | LCA Temperature (°C) | | | | | | |
| | • N (missing) | 90(0) | 244(0) | 334(0) | | | |
| | • Mean ± SD | 26.6 ± 1.5 | 29.3 ± 2.7 | 28.5 ± 2.7 | | | |
| | • Median | 26.5 | 29.4 | 28.4 | | | |
| | • Q1, Q3 | 25.9, 27.6 | 27.4, 31.2 | 26.5, 30.6 | | | |
| | • Min, Max | 22.8, 30.1 | 20.9, 35.9 | 20.9, 35.3 | | | |
| 5 | LPA Temperature (°C) | | | | | | |
| | • N (missing) | 90(0) | 244(0) | 334(0) | | | |
| | • Mean ± SD | 26.4 ± 1.8 | 29.9 ± 3.2 | 28.9 ± 3.3 | | | |
| | • Median | 26.3 | 30.3 | 28.9 | | | |
| | • Q1, Q3 | 25.4, 27.6 | 27.6, 32.4 | 26.3, 31.8 | | | |
| | • Min, Max | 21.4, 30 | 19.8, 35.9 | 19.8, 35.9 | | | |
| 6 | MCA Temperature (°C) | | | | | | |
| | • N (missing) | 90(0) | 244(0) | 334(0) | | | |
| | • Mean ± SD | 27 ± 1.5 | 29.5 ± 2.6 | 28.8 ± 2.6 | | | |
| | • Median | 27.2 | 29.6 | 28.8 | | | |
| | • Q1, Q3 | 26.1, 28 | 27.8, 31.4 | 27, 30.8 | | | |
| | • Min, Max | 23, 30.2 | 21.3, 35.1 | 21.3, 35.1 | | | |
| 7 | MPA Temperature (°C) | | | | | | |
| | • N (missing) | 90(0) | 244(0) | 334(0) | | | |
| | • Mean ± SD | 26.7 ± 1.9 | 30.1 ± 3.1 | 29.2 ± 3.2 | | | |
| | • Median | 26.7 | 30.6 | 29.2 | | | |
| | • Q1, Q3 | 25.7, 27.9 | 28, 32.3 | 26.7, 31.8 | | | |
| | • Min, Max | 21.3, 30.5 | 20.3, 36.1 | 20.3, 36.1 | | | |
| 8 | TCI Temperature (°C) | | | | | | |
| | • N (missing) | 90(0) | 244(0) | 334(0) | | | |
| | • Mean ± SD | 14 ± 12.7 | 29.7 ± 2.9 | 25.5 ± 9.9 | | | |
| | • Median | 13 | 30 | 28.7 | | | |
| | • Q1, Q3 | 1.2, 26.8 | 27.8, 31.8 | 25.8, 31.1 | | | |
| | • Min, Max | 0.12, 29.6 | 20.6, 35.5 | 0.12, 35.5 | | | |
| 9 | Outcome (%) | 90(27%) | 244(73%) | 334 | | | |

The change of focus from traditional paradigms in machine learning to Deep Learning (DL) is the product of the high accuracy achieved through its large learning structures, enabling DL to obtain deeper data traits. The need for large data size and high computational complexity can be addressed using transfer learning on pre-trained networks. Whilst it is reasonably straightforward to distinguish the foot thermogram of a control subject with a specific spatial pattern, the distribution in a diabetic foot without a specific spatial pattern is more challenging, especially as the spatial distribution may change and the detection of a temperature rise in the plantar region is important for diabetic patients.

Several studies [22,23,28–35] have attempted to extract features to identify the hot region in the plantar thermogram, to identify tissue damage or inflammation. Etehadtavakol et al. [35] proposed a method called lazy snapping to extract the extreme temperature areas in the thermogram images which can easily differentiate the coarse and fine-scale change. A thresholding method was used to identify the highest temperature areas from the plantar region [22], while Gururaj Rao et al. [34] used an active contour model of plantar segmentation and a thresholding method to extract the highest temperature points. Adam et al. [33] used Discrete Wavelet Transformation (DWT) and higher-order spectra (HOS) to derive several coefficients from the characteristics of texture and entropy. A double density-dual tree-complex wavelet transform (DD-DT-CWT) was used to decompose the image and extract several key features [32]. Saminathan et al. [31] segmented the plantar area into 11 regions using region-raising and extracted texture characteristics to classify it into a normal or ulcer group. Most of these works were reported on a small private dataset and utilized post-processing techniques, which might not be able to generalize on a different dataset and the real-time applicability and inference time were not reported. Moreover, the performance of these methods were not comparable to the machine learning based techniques.

Very few studies have applied the deep learning (DL) technique to classify thermogram images from controls and diabetic patients. Maldonado et al. [30] utilized the DL technique to segment the thermogram of the plantar area to classify ulceration or necrosis. Hernandez et al. [23] proposed a quantitative thermal change index (TCI) to measure the thermal change in the plantar region of diabetic patients to classify patients from controls. Hernandez et al. [23,29] utilized the ‘‘Plantar Thermogram Database’’ of 334-foot thermogram images and used TCI to classify subjects into Class 1 to 5 based on the spatial temperature distribution and temperature range. Cruz-Vega et al. [28] also proposed a DL technique to classify the images of the ‘‘Plantar Thermogram Database’’ into two classes at a time, but the technique is questionable as it cannot be used for clinical decision making and the applicability of such a solution for a smartphone application is not discussed.

We have utilized an available dataset to classify control and diabetic groups and developed a novel technique to automatically classify the thermogram images and compared the outcome to a 2D deep learning technique. Moreover, the light architecture and machine learning model are deployable in smartphones.

The major contributions of this paper are:

- Comparative evaluation over the state-of-the-art 2D CNN models and image enhancement techniques for the detection of diabetic foot with high accuracy.
- A detailed investigation of the relevant features to improve the detection performance when used as input to traditional classifiers.
- An investigation of feature selection and optimization techniques and classification models to maximize detection performance utilizing light classifiers.

Section II discusses the methodology, section III presents the results and discussion and section IV presents the conclusions and proposes topics for future research.

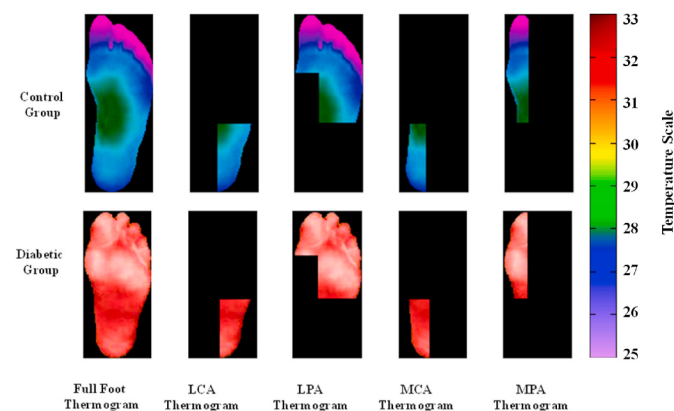


Fig. 2. Sample of MPA, LPA, MCA, and LCA angiosomes for control and diabetic foot thermogram.

2. Methodology

Fig. 1 shows the complete system block diagram. The thermogram is used as an input to extract important features, feature optimization, and ranking by different ranking techniques. The best combination of the top-ranked features was used as input to the classifier to stratify the thermogram images into diabetic and control groups. The performance of the proposed technique was compared with a 2D CNN-based image classification model for comparative evaluation. Various image enhancement techniques were utilized to enhance the 2D thermogram images and improve the performance of 2D CNN [36].

2.1. Dataset Description

A database of age, gender, height, and weight and 167-foot pair thermograms from 122 participants with diabetes mellitus and 45 controls was made public by Hernandez-Contreras et al. [29]. Continuous variables were reported with the number of missing data, median, mean, and quartiles (Q1, Q3) for diabetic and control groups (**Table 1**). The chi-square test was conducted for gender while the rank-sum test was conducted on other features. A p-value <0.05 was used as the cut-off for assessing the statistical significance [37]. All the features were of great significance as can be seen in **Table 1**, and the authors have also mentioned the exact p-value. The foot thermogram images were segmented to remove the background and were also segmented into four angiosomes for the medial plantar artery (MPA), lateral plantar artery (LPA), medial calcaneal artery (MCA), and lateral calcaneal artery (LCA) [38] (**Fig. 2**). There is a clear distinction between the thermogram images among control and diabetic patients (**Fig. 2**). In the control group, the thermogram images have a unique pattern in the temperature distribution (butterfly pattern), where the middle of the foot has higher temperature and the temperature slowly reduces in the remaining part of the foot. On the other hand, the diabetic group have comparatively higher temperature throughout the foot. The angiosome related information is not only useful to identify the arteries associated with ulceration risk but also shows the local temperature of each angiosome. Pixelated temperature readings for the full foot and the four angiosomes for both feet were available in the dataset, to encounter the problem in two dimensions: pixelated temperature and the 2D thermogram image.

2.2. Feature extraction from temperature map

Different features have been extracted by different research groups from foot thermograms over the last decade. Cajacuri et al. [39] highlighted the importance of age, gender and body mass index. Contreras et al. [29] developed the thermal change index (TCI), the mean temperature difference between the corresponding angiosomes from a

diabetic patient and a control group as shown in Equation (1).

$$TCI = \frac{CG_{ang} - DG_{ang}}{4} \quad (1)$$

where CG_{ang} and DG_{ang} are the temperature values of the angiosome for the control and diabetic groups, respectively. Barreto et al. [40] proposed features, such as Estimate temperature (ET), estimated temperature difference (ETD), and hot spot estimator (HSE) for analyzing thermograms, as shown in Equations (2)–(4).

$$ET = \frac{a_{j-1}C_{j-1} + a_jC_j + a_{j+1}C_{j+1}}{a_{j-1} + a_j + a_{j+1}} \quad (2)$$

$$ETD = |ET_{left\ Angiosome} - ET_{right\ Angiosome}| \quad (3)$$

$$HSE = |C_l - ET| \quad (4)$$

To calculate these features, the temperature map in the thermogram image is categorized into temperature classes: C_0 to C_7 . A histogram is generated for the percentage of pixels in the thermogram image, which lies in different temperature classes, where $C_0 = 26.5^\circ C$, $C_1 = 28.5^\circ C$, $C_2 = 29.5^\circ C$, $C_3 = 30.5^\circ C$, $C_4 = 31^\circ C$, $C_5 = 32.5^\circ C$, $C_6 = 33.5^\circ C$, and $C_7 = 34.5^\circ C$. The highest frequency of a temperature class is denoted by C_l and the percentage of pixels in that region is a_j . The values a_{j-1} and a_{j+1} are the percentages of pixels in the neighboring temperature classes C_{j-1} and C_{j+1} , respectively. The a_j and C_l values are used to calculate the ET of the thermogram for each angiosome which is used to calculate the ETD values. Finally, the HSE is calculated using ET and C_l values, where C_l is the highest temperature present in the angiosome regardless of its percentage in the histogram. HSE can identify severe DFU. Saminathan et al. [31] have stressed the importance of standard statistical parameters such as mean, standard deviation, and median used in various biomedical applications [41–43].

In addition to the above-mentioned features, features which are visually important to distinguish the variation in the plantar temperature distribution were formulated. Five distinct temperature ranges were found in the dataset and verified with the TCI parameters [29].

Five distinct temperature ranges were classified into normalized temperature ranges (NTR). We have computed the variable $NRT_{class\ j}$ which is the number of pixels in $class\ j$ temperature range over the total number of non-zero pixels, where $class\ j$ can be class 1 to 5. For the temperature ranges in the class, we have used the same temperature range as reported in [29].

39 features were extracted for the early detection of diabetic foot, which are age, gender, TCI, highest temperature value, NTR (Class 1–5), HSE, ET, ETD, mean, median, SD of temperature for the different angiosomes: LPA, LCA, MPA, MCA, and the full foot.

The final list of features was optimized to remove redundant features by finding the correlation between the different features. Features with more than 95% correlation were removed, which improves the overall performance by reducing the number of redundant features, avoiding overfitting [41–44].

2.3. Classification using thermogram features

Five-fold cross-validation was used in this study, where each fold was divided into a 80% training and 20% testing set. 20% of the training data

Table 2
Details of the dataset used for training, validation, and testing.

| Dataset | Class | Training Dataset Details | | | |
|-----------------------|-------|--------------------------|------------------------------|----------------------|----------------|
| | | Training Data/Fold | Augmented Training Data/Fold | Validation Data/Fold | Test Data/Fold |
| Contreras et al. [29] | DM | 190 | 1330 | 8 | 46 |
| | CG | 64 | 1664 | 4 | 22 |

was spared as the validation set. To avoid the issue of an imbalanced training dataset and biased estimates [45], Synthetic Minority Over-sampling Technique (SMOTE) [46] was used for training data augmentation.

Feature Ranking Techniques: The feature set was first optimized by removing any redundant features, i.e. features correlation more than 95% were removed. Of 39 features, after correlated feature reduction, the number of features became 28. The heatmap of the correlation matrix before and after removing the highly correlated features is presented in Fig. 3. The reduced feature set used for further investigation was: age, gender, TCI, highest temperature value, NTR (Class 1–5), HSE, ETD, STD parameters for the different angiosomes, Full Foot, and ET, mean of LPA and LCA.

The shortlisted parameters of the dataset, after optimization, were assessed to take decisions and identify the top features for binary classification. Three different sets of feature ranking were identified using the Multi-Tree Extreme Gradient Boost (XGBoost) [47], Random Forest [48], and Extra Tree [49] techniques. Default parameters were used for the feature ranking techniques to avoid overfitting, a common problem with a large number of features and a limited sample size [50,51]. The best performing top-ranked features from the different feature ranking techniques are used to identify the best combination of features using a rigorous investigation to identify the best combination of features that gave the best performance.

Classifiers: For a detailed investigation, different classifiers such as multilayer perceptron (MLP) [52], Logistic regression [53], K-Nearest Neighbor (KNN) [54], Adaboost [55], Support Vector Machine (SVM) [56], Random Forest [57], Extra Tree [58], Gradient Boosting [59], Extreme Gradient Boost (XGBoost) [60], Linear Discriminant Analysis (LDA) [61] were used. An MLP is characterized by several layers of neurons connected between the input and the output layers. MLP uses backpropagation for training the network. Logistic regression is a variant of regression function which uses a logistic function to model a binary dependent variable. While typical linear regression uses a linear relation between predictors and output, logistic regression uses a sigmoid function to relate output with linear prediction and linear prediction works like multivariate linear regression. KNN starts by determining “k”, i.e., the number of neighbors to be compared. Once the parameter “k” is determined, the object’s distance is computed with every object available in the dataset and the k-least distances were identified. XGBoost is the streamlined group calculation dependent on GBDT (Gradient Boosting Decision Tree). The principle concept of the boosting calculation is that numerous decision trees perform superior to a single one. LDA is a multi-class classification model, which can be used for dimensionality reduction. Random Forest is an ensemble of Decision Trees that combine the qualities of filter and wrapper methods. Extra Tree is a type of ensemble learning technique which aggregates the results of multiple de-correlated decision trees collected in a “forest” to output its classification result. It is similar to a Random Forest and only differs from it in the manner of construction of the decision trees in the forest. AdaBoost classifier is a meta-estimator that begins by fitting a classifier on the original dataset and then fits additional copies of the classifier on the same dataset and adjusted focusing more on difficult cases.

In this experiment, 3 feature selection techniques with 10 machine learning models were investigated with 28 optimized features to identify the best-combined results in 840 investigations.

2.4. Thermogram image classification by 2D CNNs

The application of 2D CNNs in biomedical applications is popular for automatic and early detection of abnormalities such as COVID-19 pneumonia [62–64], Tuberculosis [65], community acquired pneumonia [66], and many others [67]. As before, five-fold cross-validation is applied, i.e. the dataset is divided into five-folds, and performance metrics were reported for cumulative folds. Overall accuracy and

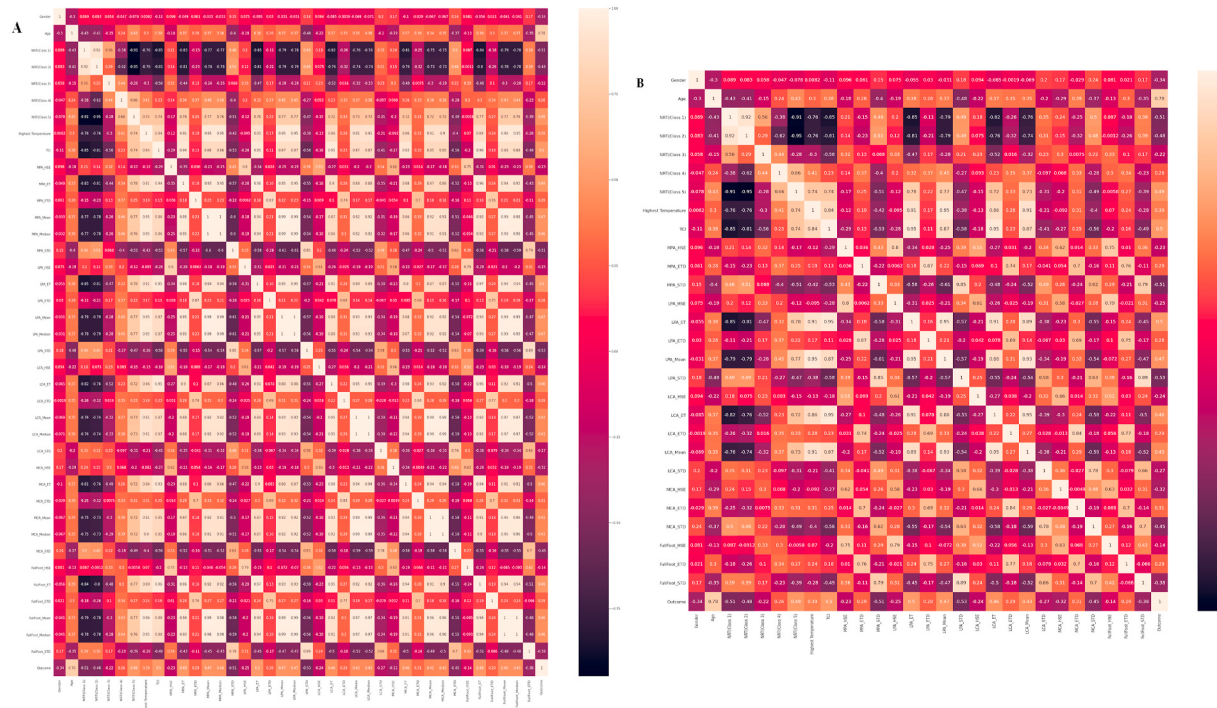


Fig. 3. Heatmap of the correlation matrix with all the features (A) and after removing the highly correlated features (B).

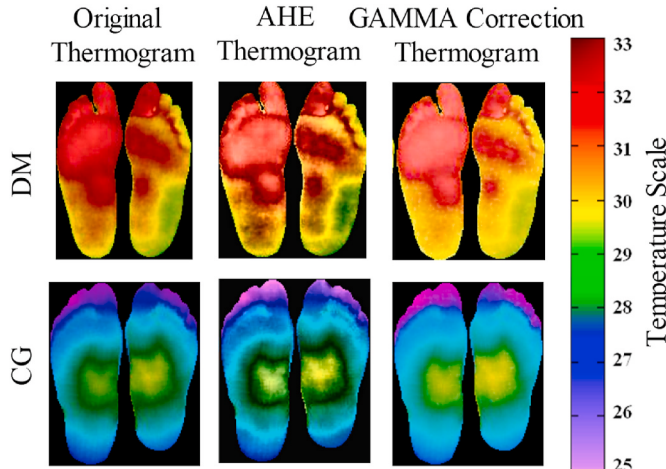


Fig. 4. Original versus enhanced thermogram images using adaptive histogram equalization (AHE) and Gamma Correction for control and diabetic foot thermograms.

weighted average of Precision, Sensitivity, Specificity, and F1-Score are reported. Since the binary class dataset is not balanced and the number of images in 80% of the dataset (training set per fold) was small. The training dataset was augmented using image rotation and translation [62–66]. The details of the training, validation and testing dataset for 2D binary classification are presented in Table 2.

Transfer Learning: Since the dataset size is small, pre-trained models, originally trained on the ImageNet database [68] were used in this study. Based on an extensive literature review and previous work [62–66], six well-known pre-trained deep learning CNNs were used in this study: ResNet18, ResNet50 [69], DenseNet201 [69], InceptionV3 [70], VGG19 [71] and MobileNetV2 [72].

Image Enhancement: Image enhancement techniques such as Histogram Equalization (HE) [73], and Adaptive Histogram Equalization (AHE), and Gamma correction [74] can help 2D CNN in classification

performances [36]. We have used the AHE technique (Fig. 3) which performs histogram equalization over small regions (i.e., patches) in the image to enhance the contrast of each region individually. It improves local contrast and edges adaptively in each region of the image to the local distribution of pixel intensities instead of the global information of the image. Gamma correction was also applied to enhance the thermogram images. It performs a non-linear operation on the source image pixels, which alternates the pixel value to improve the image using the projection relationship between the value of the pixel and the value of the gamma according to the internal map. Sample thermogram image for DM and CG patients and the enhanced images with AHE and gamma correction are shown in Fig. 4.

2.5. Performance metrics

Six performance metrics: Sensitivity, Specificity, Precision, Accuracy, F1-Score, and Area under the curve (AUC) were used as evaluation metrics where TP, FP, TN and FN are True Positive, False Positive, True Negative, and False Negative, respectively.

$$\text{Sensitivity} = \frac{(TP)}{(TP + FN)} \quad (5)$$

$$\text{Specificity} = \frac{(TN)}{(TN + FP)} \quad (6)$$

$$\text{Precision} = \frac{(TP)}{(TP + FP)} \quad (7)$$

$$\text{Accuracy} = \frac{TP + TN}{(TP + FN) + (FP + TN)} \quad (8)$$

$$\text{F1 Score} = \frac{(2 * \text{Precision} * \text{Sensitivity})}{(\text{Precision} + \text{Sensitivity})} \quad (9)$$

TP is the number of thermograms correctly identified as DM, FP is the number of incorrectly identified thermograms as DM, TN is the number of thermograms correctly classified as CG, and FN is the number of

Table 3

Performance metrics for the binary classification using a single foot thermogram using 2D CNN. The best-performing network is highlighted in bold.

| Network | Class | Accuracy (%) | Precision (%) | Sensitivity (%) | F1-score (%) | Specificity (%) | Inference time (msec) |
|-------------|---------|---------------------|---------------------|---------------------|---------------------|---------------------|-----------------------|
| MobilenetV2 | DM | 92.51 ± 5.44 | 94.69 ± 4.63 | 95.08 ± 4.47 | 94.88 ± 4.55 | 85.56 ± 7.26 | 5.252 |
| | CG | 92.51 ± 3.30 | 86.52 ± 4.29 | 85.56 ± 4.41 | 86.04 ± 4.35 | 95.08 ± 2.71 | |
| | Overall | 92.51 ± 2.82 | 92.49 ± 2.83 | 92.51 ± 2.82 | 92.50 ± 2.82 | 88.13 ± 3.47 | |
| Resnet18 | DM | 90.42 ± 6.08 | 91.41 ± 5.79 | 95.90 ± 4.10 | 93.60 ± 5.06 | 75.56 ± 8.88 | 2.545 |
| | CG | 90.42 ± 3.69 | 87.18 ± 4.19 | 75.56 ± 5.39 | 80.96 ± 4.93 | 95.90 ± 2.49 | |
| | Overall | 90.42 ± 3.16 | 90.27 ± 3.18 | 90.42 ± 3.16 | 90.19 ± 3.19 | 81.04 ± 4.20 | |
| Resnet50 | DM | 93.41 ± 5.13 | 94.05 ± 4.89 | 97.13 ± 3.45 | 95.57 ± 4.25 | 83.33 ± 7.70 | 6.164 |
| | CG | 93.41 ± 3.11 | 91.46 ± 3.51 | 83.33 ± 4.68 | 87.21 ± 4.19 | 97.13 ± 2.09 | |
| | Overall | 93.41 ± 2.66 | 93.35 ± 2.67 | 93.41 ± 2.66 | 93.32 ± 2.68 | 87.05 ± 3.60 | |
| DenseNet201 | DM | 94.01 ± 4.91 | 95.91 ± 4.11 | 95.91 ± 4.11 | 95.91 ± 4.11 | 88.89 ± 6.49 | 26.138 |
| | CG | 94.01 ± 2.98 | 88.89 ± 3.94 | 88.89 ± 3.94 | 88.89 ± 3.94 | 95.91 ± 2.49 | |
| | Overall | 94.01 ± 2.54 | 94.01 ± 2.54 | 94.01 ± 2.54 | 94.01 ± 2.54 | 90.78 ± 3.11 | |
| InceptionV3 | DM | 93.71 ± 5.02 | 93.73 ± 5.01 | 97.95 ± 2.93 | 95.79 ± 4.15 | 82.22 ± 7.90 | 15.353 |
| | CG | 93.71 ± 3.05 | 93.67 ± 3.06 | 82.22 ± 4.80 | 87.57 ± 4.14 | 97.95 ± 1.78 | |
| | Overall | 93.71 ± 2.60 | 93.71 ± 2.60 | 93.71 ± 2.60 | 93.58 ± 2.63 | 86.46 ± 3.67 | |
| VGG19 | DM | 92.22 ± 5.53 | 93.60 ± 5.06 | 95.90 ± 4.10 | 94.74 ± 4.61 | 82.22 ± 7.90 | 6.284 |
| | CG | 92.22 ± 3.36 | 88.10 ± 4.06 | 82.22 ± 4.80 | 85.06 ± 4.47 | 95.90 ± 2.49 | |
| | Overall | 92.22 ± 2.87 | 92.12 ± 2.89 | 92.21 ± 2.87 | 92.13 ± 2.89 | 85.91 ± 3.73 | |

Table 4

Performance metrics for the best performing networks using 2D CNN on different image enhancement techniques using single foot thermograms. The best-performing network is highlighted in bold.

| Enhancement Technique | Best Network | Class | Accuracy (%) | Precision (%) | Sensitivity (%) | F1-score (%) | Specificity (%) | Inference time (msec) |
|-----------------------|--------------|---------|---------------------|---------------------|---------------------|---------------------|---------------------|-----------------------|
| Original | DenseNet201 | DM | 94.01 ± 4.91 | 95.91 ± 4.11 | 95.91 ± 4.11 | 95.91 ± 4.11 | 88.89 ± 6.49 | 26.138 |
| | | CG | 94.01 ± 2.98 | 88.89 ± 3.94 | 88.89 ± 3.94 | 88.89 ± 3.94 | 95.91 ± 2.49 | |
| | | Overall | 94.01 ± 2.54 | 94.01 ± 2.54 | 94.01 ± 2.54 | 94.01 ± 2.54 | 90.78 ± 3.11 | |
| AHE | InceptionV3 | DM | 92.22 ± 5.53 | 94.67 ± 4.64 | 94.67 ± 4.64 | 94.67 ± 4.64 | 85.56 ± 7.26 | 15.450 |
| | | CG | 92.22 ± 3.36 | 85.56 ± 4.41 | 85.56 ± 4.41 | 85.56 ± 4.41 | 94.67 ± 2.82 | |
| | | Overall | 92.22 ± 2.87 | 92.22 ± 2.87 | 92.22 ± 2.87 | 92.22 ± 2.87 | 88.01 ± 3.48 | |
| Gamma Correction | InceptionV3 | DM | 93.41 ± 6.44 | 93.70 ± 6.30 | 97.54 ± 6.30 | 95.58 ± 6.30 | 82.22 ± 9.92 | 15.422 |
| | | CG | 93.41 ± 6.12 | 92.51 ± 5.30 | 82.22 ± 5.30 | 87.06 ± 5.30 | 97.54 ± 3.30 | |
| | | Overall | 93.41 ± 3.11 | 93.38 ± 3.12 | 93.41 ± 3.12 | 93.28 ± 3.12 | 86.35 ± 4.30 | |

Table 5

Performance metrics for the binary classification using Gamma enhanced dual-foot thermogram using deep CNNs. The best-performing network is highlighted in bold.

| Network | Class | Accuracy (%) | Precision (%) | Sensitivity (%) | F1-score (%) | Specificity (%) | Inference time (msec) |
|-------------|---------|---------------------|---------------------|---------------------|---------------------|---------------------|-----------------------|
| MobilenetV2 | DM | 95.81 ± 4.14 | 97.52 ± 3.21 | 96.72 ± 3.68 | 97.12 ± 3.46 | 93.33 ± 5.15 | 5.188 |
| | CG | 95.81 ± 2.51 | 91.30 ± 3.54 | 93.33 ± 3.13 | 92.30 ± 3.35 | 96.72 ± 2.23 | |
| | Overall | 95.81 ± 2.15 | 95.84 ± 2.14 | 95.81 ± 2.15 | 95.82 ± 2.15 | 94.24 ± 2.50 | |
| Resnet18 | DM | 93.41 ± 5.13 | 94.40 ± 4.75 | 96.72 ± 3.68 | 95.55 ± 4.26 | 84.44 ± 7.49 | 2.430 |
| | CG | 93.41 ± 3.11 | 90.48 ± 3.68 | 84.44 ± 4.55 | 87.36 ± 4.17 | 96.72 ± 2.23 | |
| | Overall | 93.41 ± 2.66 | 93.34 ± 2.67 | 93.41 ± 2.66 | 93.34 ± 2.67 | 87.75 ± 3.52 | |
| Resnet50 | DM | 90.42 ± 6.08 | 92.74 ± 5.36 | 94.26 ± 4.81 | 93.49 ± 5.1 | 80.00 ± 8.26 | 6.164 |
| | CG | 90.42 ± 3.69 | 83.72 ± 4.63 | 80.00 ± 5.02 | 81.82 ± 4.84 | 94.26 ± 2.92 | |
| | Overall | 90.42 ± 3.16 | 90.31 ± 3.17 | 90.42 ± 3.16 | 90.35 ± 3.17 | 83.84 ± 3.95 | |
| DenseNet201 | DM | 91.62 ± 5.72 | 92.86 ± 5.32 | 95.90 ± 4.10 | 94.36 ± 4.77 | 80.00 ± 8.26 | 25.732 |
| | CG | 91.62 ± 3.48 | 87.80 ± 4.11 | 80.00 ± 5.02 | 83.72 ± 4.63 | 95.90 ± 2.49 | |
| | Overall | 91.62 ± 2.97 | 91.50 ± 2.99 | 91.62 ± 2.97 | 91.49 ± 2.99 | 84.28 ± 3.90 | |
| InceptionV3 | DM | 93.41 ± 5.13 | 93.70 ± 5.02 | 97.54 ± 3.20 | 95.58 ± 4.25 | 82.22 ± 7.90 | 16.701 |
| | CG | 93.41 ± 3.11 | 92.50 ± 3.30 | 82.22 ± 4.80 | 87.06 ± 4.21 | 97.54 ± 1.94 | |
| | Overall | 93.41 ± 2.66 | 93.38 ± 2.67 | 93.41 ± 2.66 | 93.28 ± 2.69 | 86.35 ± 3.68 | |
| VGG19 | DM | 92.22 ± 5.53 | 92.91 ± 5.30 | 96.72 ± 3.68 | 94.78 ± 4.60 | 80.00 ± 8.26 | 6.292 |
| | CG | 92.22 ± 3.36 | 90.00 ± 3.76 | 80.00 ± 5.02 | 84.71 ± 4.52 | 96.72 ± 2.23 | |
| | Overall | 92.22 ± 2.87 | 92.13 ± 2.89 | 92.21 ± 2.87 | 92.07 ± 2.90 | 84.51 ± 3.88 | |

thermograms incorrectly identified as CG. We report the overall accuracy and weighted performance metric, with a 95% confidence interval (CI), for Sensitivity, Specificity, Precision, and F1 Score. In addition, to compare the computational complexity of the different machine learning techniques, the inference time was calculated for the best performing 2D CNN models and 1D classifiers. The models that can be deployed in a smartphone were also identified.

All the experiments were performed by a computer with the following configuration: CPU Intel i7-10750H @2.6 GHz, GPU NVIDIA GeForce RTX 2070 Super, RAM 32 GB. Matlab 2020a was used for initial pre-processing and scikit-learn and PyTorch were used for classical

machine learning and deep learning models, respectively.

3. Results and discussion

The experimental results are divided into two sections: The first section presents the foot ulcer detection results by deep CNN models with transfer learning over the pre-trained networks while exploring the effects of different image enhancement techniques on thermogram image classification. Moreover, the effect of single and dual-foot as input was investigated for binary classification. In the second section, comparative evaluations among the best-performing machine learning

Table 6

Performance metrics for the best-performing networks using 2D CNN on different image enhancement techniques of combined foot thermograms.

| Enhancement Technique | Network | Class | Accuracy | Precision | Sensitivity | F1-score | Specificity | Inference time (msec) |
|-----------------------|-------------|---------|---------------------|---------------------|---------------------|---------------------|---------------------|-----------------------|
| Original | DenseNet201 | DM | 90.72 ± 5.99 | 93.47 ± 5.10 | 93.85 ± 4.96 | 93.66 ± 5.03 | 82.22 ± 7.90 | 24.362 |
| | | CG | 90.72 ± 3.64 | 83.15 ± 4.70 | 82.22 ± 4.80 | 82.68 ± 4.75 | 93.85 ± 3.01 | |
| | | Overall | 90.72 ± 3.11 | 90.69 ± 3.12 | 90.72 ± 3.11 | 90.70 ± 3.11 | 85.35 ± 3.79 | |
| AHE | MobilenetV2 | DM | 92.22 ± 5.53 | 94.67 ± 4.64 | 94.67 ± 4.64 | 94.67 ± 4.64 | 85.56 ± 7.26 | 5.363 |
| | | CG | 92.22 ± 3.36 | 85.56 ± 4.41 | 85.56 ± 4.41 | 85.56 ± 4.41 | 94.67 ± 2.82 | |
| | | Overall | 92.22 ± 2.87 | 92.22 ± 2.87 | 92.22 ± 2.87 | 92.22 ± 2.87 | 88.01 ± 3.48 | |
| Gamma Correction | MobilenetV2 | DM | 95.81 ± 5.20 | 97.52 ± 4.04 | 96.72 ± 4.62 | 97.12 ± 4.34 | 93.33 ± 6.48 | 5.188 |
| | | CG | 95.81 ± 4.95 | 91.30 ± 6.96 | 93.33 ± 6.16 | 92.30 ± 6.58 | 96.72 ± 4.40 | |
| | | Overall | 95.81 ± 2.51 | 95.84 ± 2.51 | 95.81 ± 2.51 | 95.82 ± 2.51 | 94.24 ± 2.92 | |

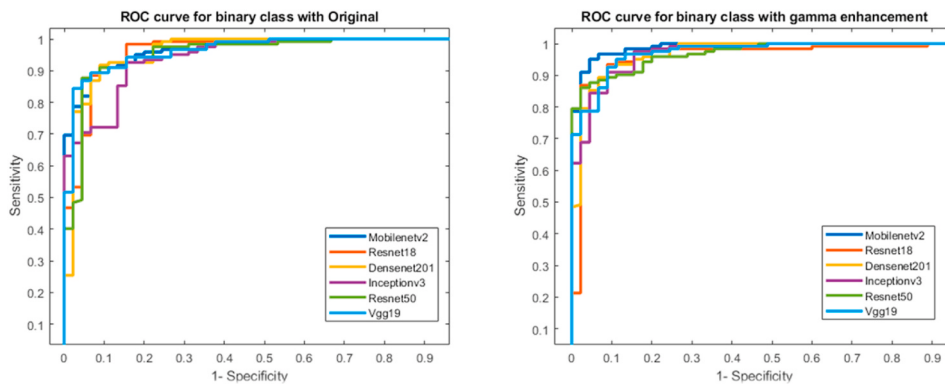


Fig. 5. ROC for the Original and Gamma Correction Enhanced thermogram using Combined Foot Thermograms.

models on the optimized thermogram features are presented.

3.1. Detection results by deep CNN models

The detection results of six deep CNN models for classifying the thermograms into control and diabetic groups from a single foot thermogram without and with image enhancement are presented in [Tables 3 and 4](#); while the data for both feet are shown in [Tables 5 and 6](#), respectively. It can be seen that the original thermograms perform better than the image enhancement techniques (AHE and Gamma) ([Table 4](#)), using the single foot thermogram. Among the six different deep CNN models investigated, DenseNet201 outperforms other networks with overall 94.01% sensitivity for the detection of DF and the class-wise sensitivities are 95.9% and 88.89% for DM and CG, respectively.

We have further investigated whether or not using a combination of foot images improves the detection performance. It was found that the Gamma enhanced dual-foot thermogram has outperformed the other methods ([Table 5](#)). Interestingly, shallow network MobilenetV2 provides the best performance with an overall 95.81% sensitivity for diabetic foot detection and the class-wise sensitivities are 96.72% and 93.33% for DM and CG, respectively.

The outperformance using a combination of foot images is explained by the fact that combined foot thermograms provide more distinguishable features which are further enhanced by the image enhancement techniques.

[Fig. 5](#) clearly shows that the utilization of Gamma enhanced thermograms improved the classification performance compared to the original thermogram images for dual-foot investigation.

3.2. Feature-based detection results

We have investigated the performance of the 10 traditional classifiers with the three feature selection techniques and different combinations of optimized features. The summary of the top-performing five combinations is presented in [Table 7](#). It can be seen that the AdaBoost Classifier with Random Forest Feature selection technique and the top

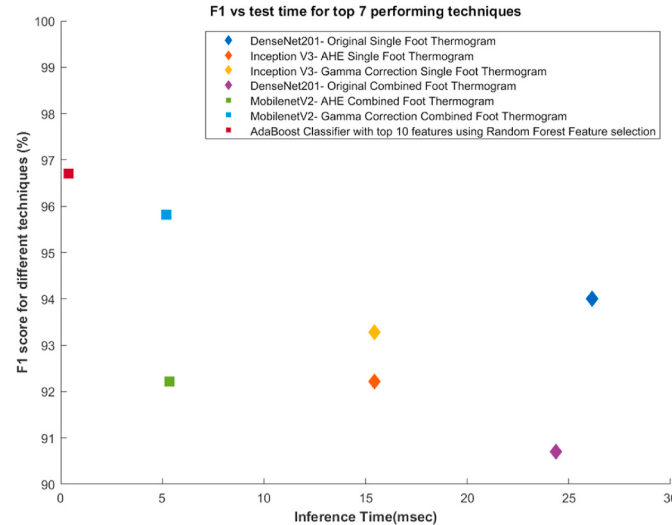


Fig. 6. Comparison of F1-score versus Inference time for the top 7 performing techniques. Note: The top-performing networks that can be deployed on smart portable devices are shown as Square blocks while Diamond blocks represent non-deployable models.

10 features shows the best performance of 96.71% sensitivity for diabetic foot detection and the class-wise sensitivities are 97.75% and 93.85% for DM and CG, respectively which is better than the top performance achieved by the deep CNN models.

[Fig. 6](#) shows the comparison of the F1-score and inference time for the top 7 performing machine learning techniques from each category-i) different image enhancement on single foot thermogram, ii) different image enhancement on combined foot thermogram, and iii) the best performing 1D classifier, respectively. Only MobileNetV2 among the CNN models and AdaBoost classifier are deployable in the mobile platform.

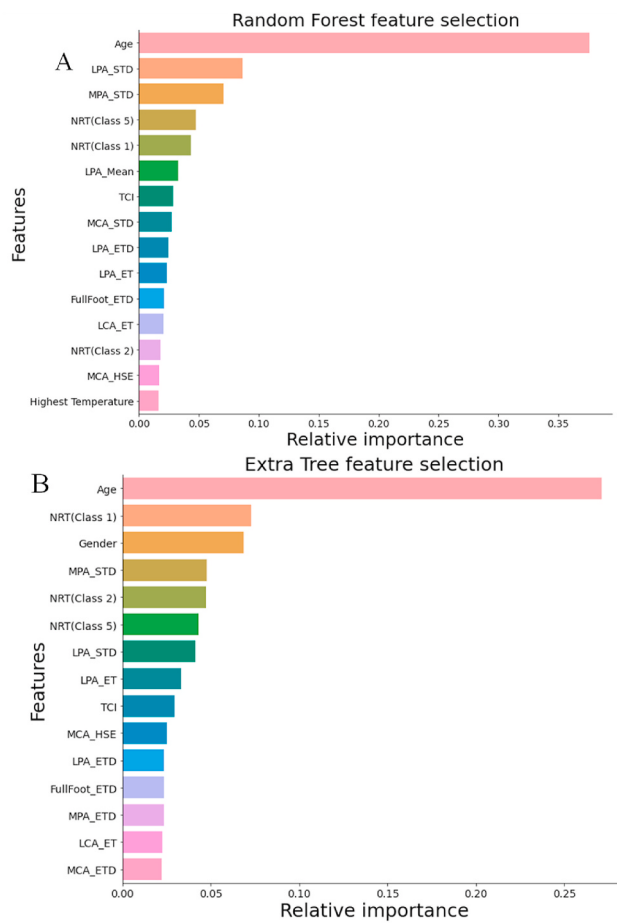


Fig. 7. Top 15 features using A) Random Forest and B) Extra Tree feature selection techniques.

To the best of the author's knowledge, this is the first detailed investigation for diabetic foot detection using deep CNN models versus traditional machine learning approaches. All possible combinations in terms of classifier and feature selection techniques, along with the ranked features were investigated. As can be seen from Table 7, the AdaBoost classifier outperforms other classifiers and the random forest feature ranking technique provides the best feature combination. The top 15 features among 28 features using Random Forest and Extra Tree feature selection techniques, after removing the highly correlated features from the initial 39 features, are shown in Fig. 7.

All the parameters are derived from temperature of the pixels in the

different angiosomes and the complete foot. As can be seen in Fig. 7 (A), the "Highest Temperature" parameter, i.e. the highest temperature pixel in the complete foot thermogram was the 15th feature according to Random Forest feature selection for classifying thermograms into Control and Diabetic groups. It is evident from Table 7 that AdaBoost with the top 10 features (Age, LPA_STD, MPD_STD, NRT (Class 1), NRT (Class 5), LPA_mean, TCI, MCA_STD, LPA_ETD, and LPA_ET) has achieved the best classification performance, which does not include 'Highest Temperature'.

This can be understood easily as the highest temperature parameter could be distinguishing feature for some patients, however, it could not be generalized for all diabetic patients. Rather Top-ranked 10 features provide better distinction among the classes.

It should be noted that the feature-based classification was done using single foot thermogram features which outperform the dual-foot approach of enhanced image thermogram using deep CNNs. However, in the feature-based approach, demographic information such as age helps to improve its performance as reported in previous work [39]. Peregrine et al. [40] have identified 11 regions of interest (ROI), which can be used to identify the diabetic foot with the help of ET, ETD, and HSE. Fig. 8 demonstrating the ROC curves for the top 1 to 10 feature

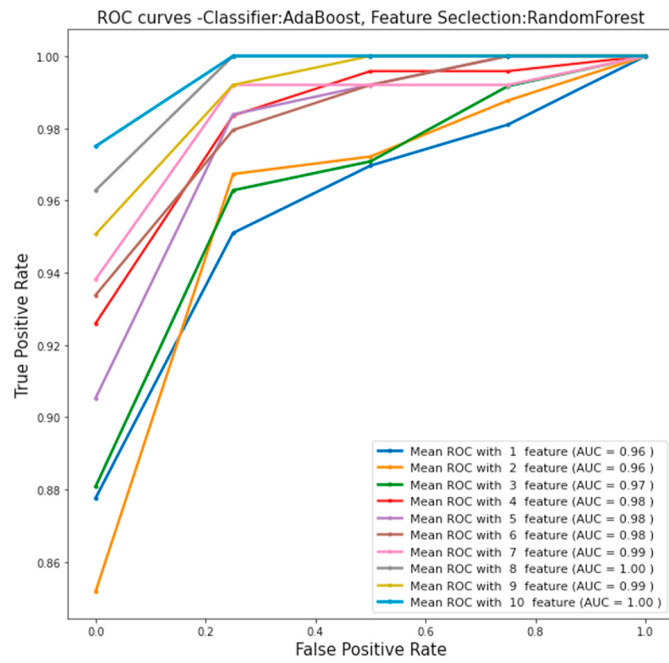


Fig. 8. ROC curves for the top 10 feature combinations.

Table 7
Performance metrics for the best-performing combinations.

| Classifier | Feature Selection | # of Feature | Class | Accuracy | Precision | Sensitivity | F1-score | Specificity | Inference time (ms) |
|------------|-------------------|--------------|---------|--------------|--------------|--------------|--------------|--------------|---------------------|
| AdaBoost | Random Forest | 10 | DM | 96.71 ± 3.69 | 97.55 ± 3.19 | 97.95 ± 2.93 | 97.75 ± 3.06 | 93.33 ± 5.15 | 0.397 |
| | | | CG | 96.71 ± 2.24 | 94.38 ± 2.89 | 93.33 ± 3.13 | 93.85 ± 3.01 | 97.95 ± 1.78 | |
| | | | Overall | 96.71 ± 1.91 | 96.70 ± 1.92 | 96.71 ± 1.91 | 96.70 ± 1.92 | 94.58 ± 2.43 | |
| AdaBoost | Extra Tree | 12 | DM | 96.41 ± 3.85 | 98.33 ± 2.64 | 96.72 ± 3.68 | 97.52 ± 3.21 | 95.56 ± 4.26 | 0.441 |
| | | | CG | 96.41 ± 2.34 | 91.49 ± 3.50 | 95.56 ± 2.59 | 93.48 ± 3.10 | 96.72 ± 2.23 | |
| | | | Overall | 96.41 ± 2.00 | 96.49 ± 1.97 | 96.41 ± 2.00 | 96.43 ± 1.99 | 95.87 ± 2.13 | |
| AdaBoost | Random Forest | 17 | DM | 96.41 ± 3.85 | 97.93 ± 2.94 | 97.13 ± 3.45 | 97.53 ± 3.21 | 94.44 ± 4.73 | 0.519 |
| | | | CG | 96.41 ± 2.34 | 92.39 ± 3.33 | 94.44 ± 2.87 | 93.41 ± 3.11 | 97.13 ± 2.09 | |
| | | | Overall | 96.41 ± 2.00 | 96.44 ± 1.99 | 96.41 ± 2.00 | 96.42 ± 1.99 | 95.17 ± 2.30 | |
| AdaBoost | Random Forest | 19 | DM | 96.41 ± 3.85 | 97.93 ± 2.94 | 97.13 ± 3.45 | 97.53 ± 3.21 | 94.44 ± 4.73 | 0.420 |
| | | | CG | 96.41 ± 2.34 | 92.39 ± 3.33 | 94.44 ± 2.87 | 93.41 ± 3.11 | 97.13 ± 2.09 | |
| | | | Overall | 96.41 ± 2.00 | 96.44 ± 1.99 | 96.41 ± 2.00 | 96.42 ± 1.99 | 95.17 ± 2.3 | |
| Extra Tree | Extra Tree | 8 | DM | 96.11 ± 4.00 | 97.93 ± 2.94 | 96.72 ± 3.68 | 97.32 ± 3.34 | 94.44 ± 4.73 | 0.299 |
| | | | CG | 96.11 ± 2.43 | 91.40 ± 3.52 | 94.44 ± 2.87 | 92.90 ± 3.22 | 96.72 ± 2.23 | |
| | | | Overall | 96.11 ± 2.07 | 96.17 ± 2.06 | 96.11 ± 2.07 | 96.13 ± 2.07 | 95.06 ± 2.32 | |

combinations also confirm that the top 10 feature combinations provided the best AUC.

As the hallux/big toe is a prominent region of interest and is in the LPA section of the foot, its contribution in the classification of the foot into diabetic and control is vital in the classification and it is natural to be included in the top 10 features. Age is a strong predictor of the diabetic foot as observed in this study [39]. Minor temperature variation is typically expected in the feet, but less variation, indicated by a lower standard deviation of temperature in LPA and MCA angiosomes, can also be an indicator of the diabetic foot. TCI is also an important indicator as it is a summary of the temperature variation in all angiosomes.

To the best of our knowledge, no previous study has reported an image enhancement effect for the detection of the diabetic foot using thermogram images. Different pre-trained networks with and without image enhancement techniques were investigated and it was found that the image enhancement techniques helped in the classification performance. The best performing Adaboost classifier can be deployed in a smartphone and can be used in the foot clinic and by users in the home setting for the early detection of DFU.

The following interesting observations can be summarized from this study:

- Gamma Correction due to its special feature enhancement has helped the network to distinguish the diabetic and control group using the dual-foot thermogram.
- A single-foot thermogram in any CNN-based classification does not improve the classification performance compared with the dual-foot approach.
- Of the various machine learning algorithms tested on the optimized feature sets the Adaboost classifier with random forest feature ranking technique outperforms all other classifiers and the 2D image-based deep learning approach.

4. Conclusion

Diabetic foot ulceration has a major impact on morbidity and mortality in patients with diabetes [5]. Early detection may help to limit DFU progression and eventually amputation. The application of artificial intelligence for early detection may have considerable utility for health care professionals, especially in primary care, and for caregivers and patients to keep track of their disease. Such online solutions become more important particularly during pandemic situations where healthcare support is drastically affected due to the burden on the healthcare system. In this study, we propose a classical machine learning-based framework for the early detection of the diabetic foot from thermogram images captured using Infra-Red (IR) cameras with a smartphone. Optimization of the thermogram features from a single foot thermogram has enabled the development of a diagnostic system that outperforms 2D image-based deep learning techniques. The proposed network can be easily deployed on a smartphone-based application and validate in a clinical trial.

Declaration of competing interests

The authors declare that they have no known competing financial interests or personal relationships that could have appeared to influence the work reported in this paper.

Acknowledgement

This work was made possible by Qatar National Research Fund (QNRF), Qatar NPRP12S-0227-190164 and International Research Collaboration Co-Fund (IRCC), Qatar grant: IRCC-2021-001 and Universiti Kebangsaan Malaysia, Malaysia under Grant DPK-2021-001. The statements made herein are solely the responsibility of the authors. Open Access publication of this article is supported by Qatar National

Library.

References

- [1] N. Cho, J. Kirigia, J. Mbanya, K. Ogurstova, L. Guariguata, W. Rathmann, IDF diabetes Atlas-8th, Int. Diabetes Federation (2015) 160.
- [2] D.S. Sims Jr., P.R. Cavanagh, J.S. Ulbrecht, Risk factors in the diabetic foot: recognition and management, Phys. Ther. 68 (12) (1988) 1887–1902.
- [3] M.M. Iversen, G.S. Tell, T. Riise, B.R. Hanestad, T. Østbye, M. Graue, et al., History of foot ulcer increases mortality among individuals with diabetes: ten-year follow-up of the Nord-Trøndelag Health Study, Norway, Diabetes Care 32 (12) (2009) 2193–2199.
- [4] A.M. Reyzelman, K. Koelewijn, M. Murphy, X. Shen, E. Yu, R. Pillai, et al., Continuous temperature-monitoring socks for home use in patients with diabetes: observational study, J. Med. Internet Res. 20 (12) (2018), e12460.
- [5] D.G. Armstrong, A.J. Boulton, S.A. Bus, Diabetic foot ulcers and their recurrence, N. Engl. J. Med. 376 (24) (2017) 2367–2375.
- [6] C.E. Ananian, Y.S. Dhillon, C.C. Van Gils, D.C. Lindsey, R.J. Otto, C.R. Dove, et al., A multicenter, randomized, single-blind trial comparing the efficacy of viable cryopreserved placental membrane to human fibroblast-derived dermal substitute for the treatment of chronic diabetic foot ulcers, Wound Repair Regen. 26 (3) (2018) 274–283.
- [7] B. Peter-Riesch, The diabetic foot: the never-ending challenge, Novelties in Diabetes 31 (2016) 108–134.
- [8] R.G. Frykberg, I.L. Gordon, A.M. Reyzelman, S.M. Cazzell, R.H. Fitzgerald, G. M. Rothenberg, et al., Feasibility and efficacy of a smart mat technology to predict development of diabetic plantar ulcers, Diabetes Care 40 (7) (2017) 973–980.
- [9] F.N. Nagase, The Impact of Diabetic Foot Problems on Health-Related Quality of Life of People with Diabetes, 2017.
- [10] R.F. van Doremalen, J.J. van Netten, J.G. van Baal, M.M. Vollenbroek-Hutten, F. van der Heijden, Infrared 3D thermography for inflammation detection in diabetic foot disease: a proof of concept, Journal of diabetes science and technology 14 (1) (2020) 46–54.
- [11] P.A. Crisologo, L.A. Lavery, Remote home monitoring to identify and prevent diabetic foot ulceration, Ann. Transl. Med. 5 (21) (2017).
- [12] J.W. Albers, R. Jacobson, Decompression nerve surgery for diabetic neuropathy: a structured review of published clinical trials, Diabetes, Metab. Syndrome Obes. Targets Ther. 11 (2018) 493.
- [13] D. Hernandez-Contreras, H. Peregrina-Barreto, J. Rangel-Magdaleno, J. Gonzalez-Bernal, Narrative review: diabetic foot and infrared thermography, Infrared Phys. Technol. 78 (2016) 105–117.
- [14] F. Ring, Thermal imaging today and its relevance to diabetes, Journal of diabetes science and technology 4 (4) (2010) 857–862.
- [15] A.W. Chan, I.A. MacFarlane, D.R. Bowsher, Contact thermography of painful diabetic neuropathic foot, Diabetes Care 14 (10) (1991) 918–922.
- [16] T. Nagase, H. Sanada, K. Takehara, M. Oe, S. Izaka, Y. Ohashi, et al., Variations of plantar thermographic patterns in normal controls and non-ulcer diabetic patients: novel classification using angiosome concept, J. Plast. Reconstr. Aesthetic Surg. 64 (7) (2011) 860–866.
- [17] T. Mori, T. Nagase, K. Takehara, M. Oe, Y. Ohashi, A. Amemiya, et al., Morphological Pattern Classification System for Plantar Thermography of Patients with Diabetes, SAGE Publications Sage CA, Los Angeles, CA, 2013.
- [18] B.F. Jones, A reappraisal of the use of infrared thermal image analysis in medicine, IEEE Trans. Med. Imag. 17 (6) (1998) 1019–1027.
- [19] N. Kaabouch, Y. Chen, J. Anderson, F. Ames, R. Paulson, Asymmetry analysis based on genetic algorithms for the prediction of foot ulcers. Visualization and Data Analysis, 2009, p. 724304, 2009.
- [20] N. Kaabouch, Y. Chen, W.-C. Hu, J.W. Anderson, F. Ames, R. Paulson, Enhancement of the asymmetry-based overlapping analysis through features extraction, J. Electron. Imag. 20 (1) (2011), 013012.
- [21] C. Liu, J.J. van Netten, J.G. Van Baal, S.A. Bus, F. van Der Heijden, Automatic detection of diabetic foot complications with infrared thermography by asymmetric analysis, J. Biomed. Opt. 20 (2) (2015), 026003.
- [22] D. Hernandez-Contreras, H. Peregrina-Barreto, J. Rangel-Magdaleno, J. Ramirez-Cortes, F. Renero-Carrillo, Automatic classification of thermal patterns in diabetic foot based on morphological pattern spectrum, Infrared Phys. Technol. 73 (2015) 149–157.
- [23] D. Hernandez-Contreras, H. Peregrina-Barreto, J. Rangel-Magdaleno, J. Gonzalez-Bernal, L. Altamirano-Robles, A quantitative index for classification of plantar thermal changes in the diabetic foot, Infrared Phys. Technol. 81 (2017) 242–249.
- [24] D.A. Hernandez-Contreras, H. Peregrina-Barreto, J.D.J. Rangel-Magdaleno, F. Orihuela-Espina, Statistical approximation of plantar temperature distribution on diabetic subjects based on beta mixture model, IEEE Access 7 (2019) 28383–28391.
- [25] P. Kamavisdar, S. Saluja, S. Agrawal, A survey on image classification approaches and techniques, International Journal of Advanced Research in Computer and Communication Engineering 2 (1) (2013) 1005–1009.
- [26] J. Ren, ANN vs. SVM: which one performs better in classification of MCCs in mammogram imaging, Knowl. Base Syst. 26 (2012) 144–153.
- [27] D. Lu, Q. Weng, A survey of image classification methods and techniques for improving classification performance, Int. J. Rem. Sens. 28 (5) (2007) 823–870.
- [28] I. Cruz-Vega, D. Hernandez-Contreras, H. Peregrina-Barreto, J.d.J. Rangel-Magdaleno, J.M. Ramirez-Cortes, Deep learning classification for diabetic foot thermograms, Sensors 20 (6) (2020) 1762.

- [29] D.A. Hernandez-Contreras, H. Peregrina-Barreto, J. de Jesus Rangel-Magdaleno, F. J. Renero-Carrillo, Plantar thermogram database for the study of diabetic foot complications, *IEEE Access* 7 (2019) 161296–161307.
- [30] H. Maldonado, R. Bayareh, I. Torres, A. Vera, J. Gutiérrez, L. Leija, Automatic detection of risk zones in diabetic foot soles by processing thermographic images taken in an uncontrolled environment, *Infrared Phys. Technol.* 105 (2020) 103187.
- [31] J. Saminathan, M. Sasikala, V. Narayananamurthy, K. Rajesh, R. Arvind, Computer aided detection of diabetic foot ulcer using asymmetry analysis of texture and temperature features, *Infrared Phys. Technol.* 105 (2020) 103219.
- [32] M. Adam, E.Y. Ng, S.L. Oh, M.L. Heng, Y. Hagiwara, J.H. Tan, et al., Automated detection of diabetic foot with and without neuropathy using double density-dual tree-complex wavelet transform on foot thermograms, *Infrared Phys. Technol.* 92 (2018) 270–279.
- [33] M. Adam, E.Y. Ng, S.L. Oh, M.L. Heng, Y. Hagiwara, J.H. Tan, et al., Automated characterization of diabetic foot using nonlinear features extracted from thermograms, *Infrared Phys. Technol.* 89 (2018) 325–337.
- [34] S.B. Gururaj Rao, U. Venkatappa, J.M. Shivaram, M.Y. Sikandar, A. Al Amoudi, Infrared thermography and soft computing for diabetic foot assessment, *Machine Learning in Bio-Signal Analysis and Diagnostic Imaging*, Elsevier, 2019, pp. 73–97.
- [35] M. Etehad tavakol, Z. Emrani, E.Y.K. Ng, Rapid extraction of the hottest or coldest regions of medical thermographic images, *Med. Biol. Eng. Comput.* 57 (2) (2019) 379–388.
- [36] A. K. Tawsifur Rahman, Yazan Qiblawey, Anas Tahir, Serkan Kiranyaz, Saad, M. T. I. Bin Abul Kashem, Somaya Al Maadeed, Susu M Zughayer, and M. E. H. C. Muhammad Salman Khan, "Exploring the effect of image enhancement techniques on COVID-19 detection using chest X-rays images" arxiv preprint arXiv: 2012.02238, 2020, 2020).
- [37] T. Dahiru, P-value, a true test of statistical significance? A cautionary note, *Ann. Ib. Postgrad. Med.* 6 (1) (2008) 21–26.
- [38] G.I. Taylor, J.H. Palmer, Angiosome theory, *Br. J. Plast. Surg.* 45 (4) (1992) 327–328.
- [39] L.A.V. Cajacuri, Early Diagnostic of Diabetic Foot Using Thermal Images, 2013.
- [40] H. Peregrina-Barreto, L.A. Morales-Hernandez, J. Rangel-Magdaleno, J.G. Avina-Cervantes, J.M. Ramirez-Cortes, R. Morales-Caporal, Quantitative estimation of temperature variations in plantar angiosomes: a study case for diabetic foot, *Computational and mathematical methods in medicine* 2014 (2014) 1–10.
- [41] M.E. Chowdhury, K. Alzoubi, A. Khandakar, R. Khallifa, R. Abouhasera, S. Koubaa, et al., Wearable real-time heart attack detection and warning system to reduce road accidents, *Sensors* 19 (12) (2019) 2780.
- [42] M.E. Chowdhury, A. Khandakar, K. Alzoubi, S. Mansoor, A. M Tahir, M.B.I. Reaz, et al., Real-time smart-digital stethoscope system for heart diseases monitoring, *Sensors* 19 (12) (2019) 2781.
- [43] M.H. Chowdhury, M.N.I. Shuzan, M.E. Chowdhury, Z.B. Mahbub, M.M. Uddin, A. Khandakar, et al., Estimating Blood pressure from the photoplethysmogram signal and demographic features using machine learning techniques, *Sensors* 20 (11) (2020) 3127.
- [44] M.A. Hall, Correlation-based feature selection for machine learning, 1999.
- [45] H. Han, W.-Y. Wang, B.-H. Mao, Borderline-Smote, A new over-sampling method in imbalanced data sets learning, *International Conference on Intelligent Computing*, 2005, pp. 878–887.
- [46] N.V. Chawla, K.W. Bowyer, L.O. Hall, W.P. Kegelmeyer, SMOTE: synthetic minority over-sampling technique, *J. Artif. Intell. Res.* 16 (2002) 321–357.
- [47] T. Chen, T. He, M. Benesty, V. Khotilovich, Y. Tang, Xgboost: extreme gradient boosting, in: R Package Version 0, vols. 4–2, 2015, pp. 1–4.
- [48] Y. Saeyts, T. Abeel, Y. Van de Peer, Robust feature selection using ensemble feature selection techniques, *Joint European Conference on Machine Learning and Knowledge Discovery in Databases*, 2008, pp. 313–325.
- [49] M. Petković, D. Kocev, S. Džeroski, Feature ranking for multi-target regression, *Mach. Learn.* 109 (6) (2020) 1179–1204.
- [50] L. Yan, H.-T. Zhang, J. Goncalves, Y. Xiao, M. Wang, Y. Guo, et al., An interpretable mortality prediction model for COVID-19 patients, *Nature Machine Intelligence* (2020) 1–6.
- [51] W. Li, Y. Yin, X. Quan, H. Zhang, Gene expression value prediction based on XGBoost algorithm, *Front. Genet.* 10 (2019) 1077.
- [52] Multilayer perceptron [Online]. Available:[2nd March], https://en.wikipedia.org/wiki/Multilayer_perceptron, 2021.
- [53] Logistic regression, Available:[2nd March], https://en.wikipedia.org/wiki/Logistic_regression, 2021.
- [54] G. Guo, H. Wang, D. Bell, Y. Bi, K. Greer, KNN model-based approach in classification, *OTM Confederated International Conferences" on the Move to Meaningful Internet Systems*, 2003, pp. 986–996.
- [55] T.-K. An, M.-H. Kim, A new diverse AdaBoost classifier, 2010, pp. 359–363. *International conference on artificial intelligence and computational intelligence*, 2010.
- [56] S.S. Keerthi, S.K. Shevade, C. Bhattacharyya, K.R.K. Murthy, Improvements to Platt's SMO algorithm for SVM classifier design, *Neural Comput.* 13 (3) (2001) 637–649.
- [57] M. Pal, Random forest classifier for remote sensing classification, *Int. J. Rem. Sens.* 26 (1) (2005) 217–222.
- [58] A. Sharaf, H. Gupta, Extra-tree classifier with metaheuristics approach for email classification, *Advances in Computer Communication and Computational Sciences*, Springer, 2019, pp. 189–197.
- [59] N. Chakrabarty, T. Kundu, S. Dandapat, A. Sarkar, D.K. Kole, Flight arrival delay prediction using gradient boosting classifier, *Emerging Technologies in Data Mining and Information Security*, Springer, 2019, pp. 651–659.
- [60] V. Bobkov, A. Bobkova, S. Porshnev, V. Zuzin, The application of ensemble learning for delineation of the left ventricle on echocardiographic records, 2016, pp. 1–5. *Dynamics of Systems, Mechanisms and Machines (Dynamics)*, 2016.
- [61] Q. Gu, Z. Li, J. Han, Linear discriminant dimensionality reduction, *Joint European Conference on Machine Learning and Knowledge Discovery in Databases*, 2011, pp. 549–564.
- [62] M. E. Chowdhury, T. Rahman, A. Khandakar, R. Mazhar, M. A. Kadir, Z. B. Mahbub, et al., "Can AI help in screening viral and COVID-19 pneumonia?", *arXiv preprint arXiv:2003.13145*, 2020.
- [63] T. Rahman, A. Khandakar, Y. Qiblawey, A. Tahir, S. Kiranyaz, S. B. A. Kashem, et al., "Exploring the effect of image enhancement techniques on COVID-19 detection using chest X-rays images," *arXiv preprint arXiv:2012.02238*, 2020.
- [64] A. Tahir, Y. Qiblawey, A. Khandakar, T. Rahman, U. Khurshid, F. Musharavati, et al., "Coronavirus: comparing COVID-19, SARS and MERS in the eyes of AI," *arXiv preprint arXiv:2005.11524*, 2020.
- [65] T. Rahman, A. Khandakar, M.A. Kadir, K.R. Islam, K.F. Islam, R. Mazhar, et al., Reliable Tuberculosis detection using chest X-ray with deep learning, segmentation and visualization, *IEEE Access* 8 (2020) 191586–191601.
- [66] T. Rahman, M.E. Chowdhury, A. Khandakar, K.R. Islam, K.F. Islam, Z.B. Mahbub, et al., Transfer learning with deep convolutional neural network (CNN) for pneumonia detection using chest X-ray, *Appl. Sci.* 10 (9) (2020) 3233.
- [67] S.M. Anwar, M. Majid, A. Qayyum, M. Awais, M. Alnowami, M.K. Khan, Medical image analysis using convolutional neural networks: a review, *J. Med. Syst.* 42 (11) (2018) 226.
- [68] J. Deng, W. Dong, R. Socher, L.-J. Li, K. Li, L. Fei-Fei, Imagenet: a large-scale hierarchical image database, 2009, pp. 248–255. *IEEE conference on computer vision and pattern recognition*, 2009.
- [69] M. Mishra, H. Menon, A. Mukherjee, Characterization of \$ S_1 \$ and \$ S_2 \$ heart sounds using stacked Autoencoder and convolutional neural network, *IEEE Transactions on Instrumentation and Measurement* 68 (9) (2018) 3211–3220.
- [70] C. Szegedy, V. Vanhoucke, S. Ioffe, J. Shlens, Z. Wojna, Rethinking the inception architecture for computer vision, *Proceedings of the IEEE Conference on Computer Vision and Pattern Recognition*, 2016, pp. 2818–2826.
- [71] K. Simonyan and A. Zisserman, "Very deep convolutional networks for large-scale image recognition," *arXiv preprint arXiv:1409.1556*, 2014).
- [72] M. Sandler, A. Howard, M. Zhu, A. Zhmoginov, L.-C. Chen, MobilenetV2: inverted residuals and linear bottlenecks, *Proceedings of the IEEE Conference on Computer Vision and Pattern Recognition*, 2018, pp. 4510–4520.
- [73] M. Veluchamy, B. Subramani, Image contrast and color enhancement using adaptive gamma correction and histogram equalization, *Optik* 183 (2019) 329–337.
- [74] J.B. Zimmerman, S.M. Pizer, E.V. Staab, J.R. Perry, W. McCartney, B.C. Brenton, An evaluation of the effectiveness of adaptive histogram equalization for contrast enhancement, *IEEE Trans. Med. Imag.* 7 (4) (1988) 304–312.